Climate Dynamics manuscript No.
(will be inserted by the editor)

Are the Teleconnections of Central Pacific and Eastern Pacific El Niño Distinct in Boreal Wintertime?

C. I. Garfinkel · M. M. Hurwitz · D. W. Waugh · A. H. Butler

Received: date / Accepted: date

Abstract A meteorological reanalysis dataset and experiments of the Goddard Earth Observing System Chemistry-Climate Model, Version 2 (GEOS V2 CCM) are used to study the boreal winter season teleconnections in the Pacific-North America region and in the stratosphere generated by Central Pacific and Eastern Pacific El Niño. In the reanalysis data, the sign of the North Pacific and stratospheric response to Central Pacific El Niño is sensitive to the composite size, the

C. I. Garfinkel

Department of Earth and Planetary Science, Johns Hopkins University, Baltimore, MD 21209.

E-mail: cig4@jhu.edu

M. M. Hurwitz

NASA Goddard Earth Sciences Technology and Research (GESTAR), Morgan State University, Baltimore, MD, USA and NASA Goddard Space Flight Center, Greenbelt, MD, USA

D. W. Waugh

Department of Earth and Planetary Science, Johns Hopkins University, Baltimore, MD 21209

A. H. Butler

Climate Prediction Center, NCEP, NOAA, Camp Springs, Maryland, USA

specific Central Pacific El Niño index used, and the month or seasonal average that is examined, highlighting the limitations of the short observational record. Long model integrations suggest that the response to the two types of El Niño are similar in both the extratropical troposphere and stratosphere. Namely, both Central Pacific and Eastern Pacific El Niño lead to a deepened North Pacific low and a weakened polar vortex, and the effects are stronger in late winter than in early winter. However, the long experiments do indicate some differences between the two types of El Niño events regarding the latitude of the North Pacific trough, the early winter polar stratospheric response, surface temperature and precipitation over North America, and globally averaged surface temperature. These differences are generally consistent with, though smaller than, those noted in previous studies.

Keywords Central Pacific ENSO · Teleconnections · Stratospheric Dynamics

1 Introduction

The El Niño - Southern Oscillation (ENSO) is the dominant mode of interannual variability in the Tropics, and it has well-known teleconnections into the Northern Hemisphere (NH) midlatitudes [Horel and Wallace, 1981, Ropelewski and Halpert, 1987, Trenberth and Caron, 2000]. These teleconnections have been able to provide a foundation for regional seasonal forecasts [Shukla et al., 2000, Barnston et al., 2005]. ENSO also has a well known impact on globally averaged surface temperature [Halpert and Ropelewski, 1992, Kumar et al., 1994, Mann and Park, 1994]. Recently, these teleconnections into the midlatitudes, and in particular in the tropospheric North Pacific region (NP), have been shown to influence the wintertime NH stratospheric polar vortex. Specifically, a deepened low in the NP is thought to enhance planetary-scale waves in the troposphere, and the enhanced waves then propagate vertically into the stratosphere where they break and subsequently weaken the polar vortex [Garfinkel and Hartmann, 2008, Garfinkel et al., 2010, Nishii et al., 2010]. This mechanism appears to explain the weakening of the vortex observed during canonical El Niño events in which warm sea surface temperature anomalies (SSTa) are present in the equatorial East Pacific [Manzini et al., 2006, Garfinkel and Hartmann, 2007, Cagnazzo et al., 2009, Bell et al., 2009, Ineson and Scaife, 2009]. This variant of El Niño will be referred to as EPW, or East Pacific warming, in the rest of this manuscript. Anomalously cold sea surface temperatures in this region (i.e. La Niña, or LN) force a largely opposite response in the extratropics [Hoerling et al., 1997].

More recently, a second mode of variability in the Tropical Pacific Ocean has been identified. While EPW events manifest as a region of warm SSTa concentrated in the East Pacific, this new mode of variability consists of warm SSTa concentrated in the central Pacific (CPW, or central Pacific warming; Trenberth and Stepaniak [2001]). Much recent attention has focused on the relationship between this new mode of variability and EPW and on the possibility that this mode of variability is excited by climate change[Yeh et al., 2009]. This mode of variability has been referred to as "dateline El Niño", "Central Pacific El Niño", "El Niño Modoki", or "Warm Pool El Niño" [Larkin and Harrison, 2005, Yu and Kao, 2007, Ashok et al., 2007, Kug et al., 2009, Kao and Yu, 2009]. Although the aforementioned studies used different names and emphasized somewhat different aspects of these El Niño events, they appear to be examining very similar phenomena.

Several recent papers have commented on the nature of the CPW effects in the NH extratropical upper troposphere and stratosphere but find apparently contradictory results. Hegyi and Deng [2011] find that CPW leads to an anomalous ridge (i.e. opposite to EPW) over the NP - a region strongly linked to wave driving of the polar vortex - and a stronger stratospheric vortex. Xie et al. [2012] also find that CPW leads to a strengthened vortex. In contrast, Graf and Zanchettin [2012] find that CPW leads to a stronger trough in the NP than EPW, but that both lead to a weaker stratospheric vortex. This discrepancy impacts the surface climate response to CPW as well: the extratropical surface climate anomalies in the CPW composites from each of these studies differ qualitatively. Hegyi and Deng [2011] associate CPW with the positive phase of the Arctic Oscillation (AO), while Graf and Zanchettin [2012] associate it with the negative phase of the North Atlantic Oscillation (NAO). All of these studies rely on reanalysis data, and it is not clear whether the limited length of the observational record might result in aliasing of unrelated variability. It is therefore not clear whether (and in what ways) CPW teleconnections differ from EPW teleconnections.

Model simulations are therefore essential for understanding (potential) differences between CPW and EPW teleconnections. In model experiments, Zubiaurre and Calvo [2012] find that CPW leads to a deepened NP low in late-winter (though the stratospheric polar vortex response is not robust), while Xie et al. [2012] find that the sign of the NH polar stratospheric response to CPW depends on the Quasi-Biennial Oscillation (QBO). However, unrelated externally forced variability is present in the experiments of Zubiaurre and Calvo [2012] (or in any experiment forced by historical conditions), and the 30-year long experiments of Xie et al. [2012] are potentially too short to differentiate between the phases of the QBO.

The goal of this study is to better understand the degree of difference between CPW and EPW teleconnections in the surface and upper tropospheric Pacific-North America region and in the stratosphere in boreal winter. Section 2 will introduce the data used in this study. Section 3 will revisit the teleconnections of CPW in the reanalysis record. We will show that the discrepancy between Hegyi and Deng [2011] and Graf and Zanchettin [2012] can be traced back to their individual definitions of CPW, and thus to the sets of winters composited to represent the CPW phenomenon. The stratospheric response to a wide range of CPW indices will then be objectively inter-compared. We will show that commonly used CPW indices are not interchangeable. The magnitude and sign of the NP and stratospheric responses depends on the month or seasonal average that is examined, the index chosen, and the number of events composited. Section 4 will show that in 50-year long perpetual ENSO GEOSCCM experiments, CPW and EPW lead to generally similar teleconnections in the Pacific-North America region, but that differences between CPW and EPW in this region (where they exist) are consistent with previous studies. Section 4 will also show that CPW and EPW lead to similar polar vortex responses in late winter. Finally, Section 5 will consider the minimum number of CPW events necessary before robust conclusions can be drawn regarding the nature of CPW teleconnections.

2 Data and Methodology

2.1 Reanalysis

The 12 UTC data produced by the European Center for Medium-Range Weather Forecasts (ECMWF) is used. The ERA-40 dataset is used for the first 44 years

[Uppala et al., 2005], and the analysis is extended by using operational ECMWF analysis. All relevant data from the period September 1958 to August 2007 are included in this analysis, yielding 49 years of data. Note that when we restrict our composites to include the satellite era only or use NASA's Modern-Era Retrospective Analysis for Research and Applications [MERRA, Rienecker et al., 2011] reanalysis, we find similar results.

Section 3 will examine the NP and polar vortex response to a wide range of ENSO indices in order to test sensitivity to EPW and CPW definition. The indices are: (1) Niño1+2, (2) Niño3.4, (3) El Niño Modoki [Ashok et al., 2007], (4) SSTa in the region 10°S-15°N, 165°E-130°W [as in section 3.3 of Hegyi and Deng, 2011], (5) 1.5×Niño4-0.5×Niño3, (6) and events in which both the Niño4 index and Niño3 index exceed 0.5K but the Niño4 index exceeds the Niño3 index. The last four are nominally CPW indices. While additional CPW definitions exist (and have been explored), the definitions we chose are sufficient to demonstrate the sensitivity of the response to CPW index. The Niño1+2, Niño3.4, and Niño4 indices are from the CPC/NCEP
`http://www.cpc.ncep.noaa.gov/data/indices/ersst3b.nino.mth.ascii`. Other indices are computed from the HadISST1 SST [Rayner et al., 2003].

Table 1 lists the six most extreme winters (defined by the NDJFM average) as defined by each index. The SSTa associated with the ENSO definitions are presented graphically in Figure 1. Figure 1a and 1b show the SSTa during the six strongest EPW events; note that the years chosen (and thereby the SST anomalies) for these two composites are very similar. Figure 1c-g shows the SSTa during extreme CPW events; warm SSTa are present in the Central Pacific in all cases, though tropical SST anomalies vary between and within the CPW composites. The

ENSO indices, Reanalysis

ENSO index	definition	boreal winters	references
Niño1+2	0-10°S, 90°W-80°W	72/73, 82/83, 86/87, 91/92, 97/98, 02/03	NOAA/CPC
Niño3.4	5°N-5°S, 170°-120°W	65/66, 72/73, 82/83, 86/87, 91/92, 97/98	NOAA/CPC
Modoki	SSTA-SSTB/2-SSTC/2, where SSTA averages over 165°E-140°W, 10°S-10°N, SSTB averages over 110°W-70°W, 15°S-5°N, and SSTC 125°E- 145°E, 10°S-20°N	67/68, 68/69, 77/78, 90/91, 91/92, 94/95	Ashok et al. [2007], Zubiaurre and Calvo [2012]
HegyiDeng	10°S-15°N, 165°E-130°W	68/69, 82/83, 87/88, 94/95, 97/98, 02/03	Hegyi and Deng [2011]
1.5N4-0.5N3	1.5*SSTA-0.5*SSTB, where SSTA is Niño4 and SSTB is Niño3 (5°N-5°S, 150°W-90°W)	68/69, 90/91, 94/95, 02/03, 04/05, 06/07	similar to Trenberth and Stepaniak [2001], Ren and Jin [2011]
Nin4>Nin3	years in which both Niño4 and Niño3 exceed 0.5C, and in which Niño4 is greater than Niño3	68/69, 90/91, 94/95, 96/97, 01/02, 04/05	similar to Hurwitz et al. [2011a,b]

Table 1 ENSO indices examined in the inter-comparison of ENSO teleconnections in Section 3. The first two are nominally EPW composites, and the rest are nominally CPW composites. Note that the six strongest El Niño years as given by Niño3 and Niño1+2 are identical; we therefore choose Niño3.4 as the second EPW definitions. Also note that the reference(s) do not necessarily examine the events listed here, either because their period of record was different (here we focus on 1958/1959 to 2006/2007) or because fewer or more than six events were chosen. The procedure adopted by Graf and Zanchettin [2012] to identify CPW years cannot be summarized by a single index.

six winters chosen are listed on each plot. By compositing these winters together and comparing the responses among the composites, we will assess the sensitivity of El Niño teleconnections to the El Niño definition.

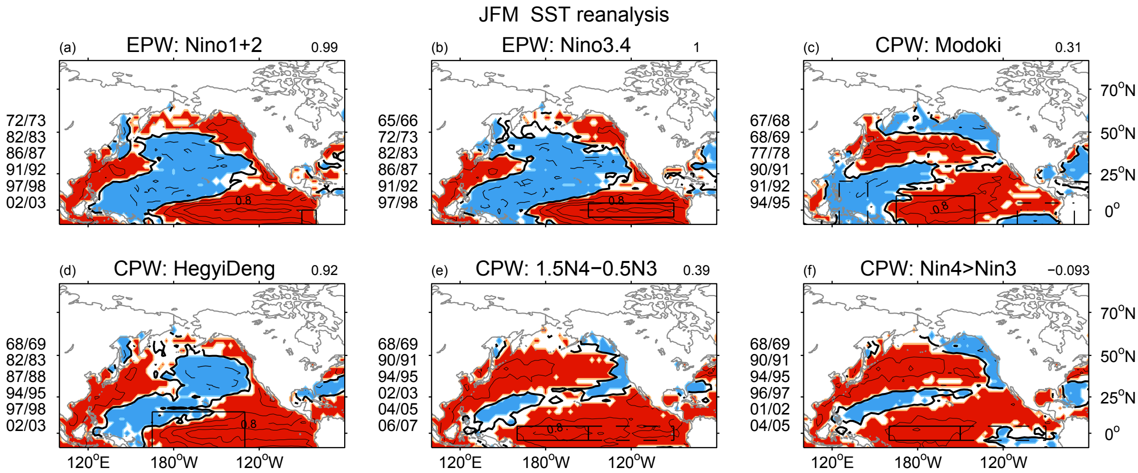

Fig. 1 Sea surface temperature (SST) anomalies in late winter associated with each composite of ENSO events. Contours are shown at ±0.4, ±0.8, ±1.2, ±2, and ±3K. Anomalies greater than 0.1K are shaded. The pattern correlation between the SSTa in the Niño3.4 composite and the SSTa in the other composites are shown. Boxes indicate the region in which SSTa have been averaged. The HadISST1 SST [Rayner et al., 2003] are used to display the SSTa associated with each composite.

2.2 GEOSCCM

We examine four 50-yr time-slice simulations forced by repeating annual cycles of sea surface temperatures and sea ice that represent CPW, EPW and neutral ENSO events, and they are referred to as CPW, EPW, NTRL, and CPWideal. The CPW and NTRL experiments are the same experiments analyzed in Hurwitz et al. [2011b], and the EPW experiment is described in Garfinkel et al. [2012a]. The SSTa used to force the simulations are shown in Figure 2. The CPW SSTa peaks in the Central Pacific while the EPW SSTa peaks in the Eastern Pacific, and the magnitude of the peak SSTa used to drive the EPW and CPW experiments differs by nearly a factor of two. This difference in magnitude of the peak equatorial SSTa is true of observed EPW and CPW events (cf. Figure 1 and Figure 13 of Kao and Yu [2009]). The rapid decrease in SSTa in the spring following an EPW event evident in Figure 2a,d is also realistic (cf. Figure 13 of Kao and Yu [2009]). The SSTa are stronger than in an average EPW or CPW event, but they are within the observational range (not shown). A second, idealized CPW experiment is also analyzed and is referred to as CPWideal. In CPWideal, SSTa are identically zero poleward of 20N and 20S, east of America, and west of 115E (i.e. outside of the tropical Pacific). Between 10S and 10N, 140E and 120W (i.e. in the deep tropical central Pacific), the SSTa are identical to that in the CPW experiment. In between, the SSTs are a linear interpolation between the NTRL and CPW SSTs, except that anomalously cold SSTa are included in the far-Eastern Pacific (see Figure 2c,f). A separate experiment identical to CPWideal but without cold SSTa in the Eastern Pacific was performed, and the results are nearly identical. The CPWideal experiment isolates the impact of postive SST anomalies in the central equatorial Pacific. Finally, we have performed a perpetual LN experiment, and the extratropical response is nearly equal in magnitude and opposite in pattern and sign [not shown, but see Garfinkel et al., 2012a]. Each SST composite spans from the July preceding the SONDJF peak in tropical SSTa through June of the following year. The key point is that the model integrations provide many samples of the atmospheric response to SSTa, and are long enough to achieve statistical robustness.

Hurwitz et al. [2011b] describes the model formulation in detail. Briefly, the GEOS V2 CCM couples the GEOS-5 atmospheric general circulation model (GCM) with a comprehensive stratospheric chemistry module. The model has 2° latitude x 2.5° longitude horizontal resolution and 72 vertical layers, with a model top at 0.01 hPa. Greenhouse gas and ozone-depleting substance concentrations represent the year 2005. Variability related to the solar cycle and volcanic aerosols are not considered. The model internally generates a QBO. Experiments with a global coupled ocean or a mixed-layer ocean outside of the deep Tropics may be explored in the future. This version of GEOSCCM is related to the GEOS-5 AGCM that is used for operational seasonal forecasting. SPARC-CCMVal [2010] grades highly the representation of the Northern Hemisphere stratosphere by the GEOSCCM as compared to the multi-model mean and observations.

Details of the biases in GEOSCCM's ENSO teleconnections can be found in Garfinkel et al. [2012a]. Briefly, Garfinkel et al. [2012a] show that the representation of El Niño teleconnections in GEOSCCM when forced with observed SSTs is generally comparable to that in five other chemistry climate models and in reanalysis data.

2.3 Methodology

Monthly mean values are examined for both data sources. For the reanalysis, the climatological monthly means were subtracted to generate anomalies. For GEOSCCM, the monthly means from the NTRL integration were subtracted from the CPW and EPW integrations to generate anomalies. We also show EPW-CPW differences in order to highlight differences between their teleconnections. The Student's-t difference of means test is used throughout to ascertain significance.

Our 50-year GEOSCCM integrations are long enough to meaningfully analyze differences between months within the extended winter season and between

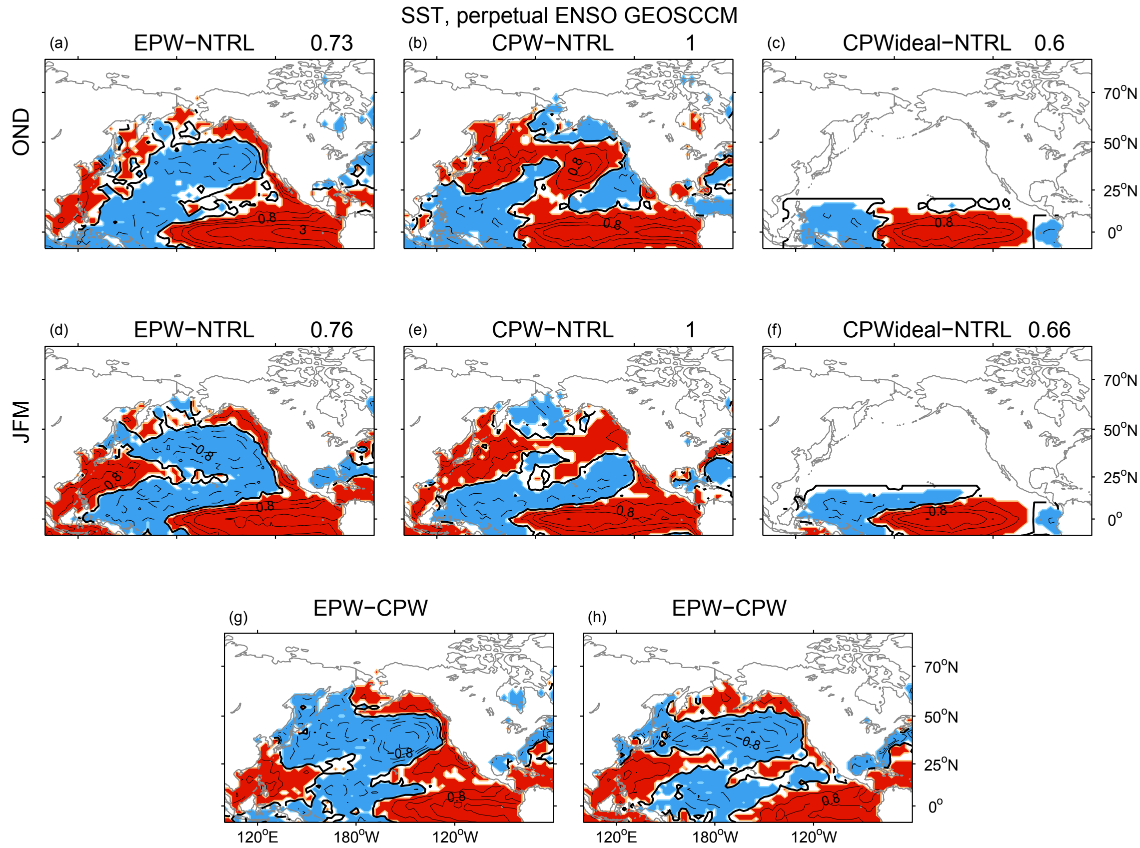

Fig. 2 Sea surface temperatures (SST) used to force the perpetual ENSO GEOSCCM integrations, as compared to the neutral ENSO experiment. Contours are shown at ±0.4, ±0.8, ±1.2, ±2, and ±3K. Anomalies greater than 0.1K are shaded. (a)-(c) and (g) are for early winter (OND) and (d)-(f) and (h) are for late winter. (g),(h) compare the EPW and CPW integrations. The pattern correlation between the CPW and EPW anomalies are shown for (a-f).

EPW and CPW. Appendix A demonstrates that the 300hPa height anomalies in GEOSCCM are weaker in early winter than in late winter (cf. Frederiksen and Branstator [2005]). Motivated by this model finding, we composite the response in early winter (October, November, and December; OND) separately from the response in late winter (January, February, and March; JFM) in Section 3 and 4.

For the reanalysis, we focus on two diagnostics: height anomalies at 300hPa and polar cap height anomalies area-weighted from 70N and poleward. For GEOSCCM, we also show the precipitation anomalies, sea level pressure anomalies, and surface temperature anomalies in the Pacific-North America region in order to provide context for the upper tropospheric and stratospheric response. Finally, we also discuss the surface temperature response in the European sector (i.e. NAO) and in the global average.

3 Sensitivity to ENSO Composite Definition: Reanalysis Data Revisited

We first consider the robustness of the response to CPW and EPW in the reanalysis record. There is no consensus on the Arctic response to CPW events in the recent literature. Hegyi and Deng [2011] and Xie et al. [2012] find that CPW leads to an anomalous ridge (as opposed to an anomalous trough in EPW) over the NP region most strongly linked to wave driving of the polar vortex, and a stronger stratospheric vortex. In contrast, Graf and Zanchettin [2012] find that CPW leads to a stronger trough in the NP than EPW, but that both lead to a weaker stratospheric vortex. The discrepancy between these studies can be traced back to their individual definitions of CPW, and thus to the sets of winters composited to represent the CPW phenomenon. Namely, both Graf and Zanchettin [2012] and Hegyi and Deng [2011] include the winters of 94/95 and 02/03 as CPW, yet the choice of the other winters included in the CPW composites differ. Hegyi and Deng [2011] include 2004/2005 which had a strong vortex. In contrast, Graf and Zanchettin [2012] do not include 2004/2005 but they do include 1968/1969 and 1986/1987 which had warm vortices. All three of these winters were El Niño, but it appears that subjective decisions on what El Niño winters are considered CPW has significantly impacted the ultimate conclusion of each study and can explain the differences between these studies. We therefore explore sensitivity to CPW definition by objectively inter-comparing the extratropical response in an ensemble of ENSO composites. We will show that commonly used ENSO indices, and in particular CPW indices, are not interchangeable.

Our specific methodology is as follows. The six most extreme winters as identified by six different ENSO definitions are composited (see Section 2). We then compare the 300hPa height anomalies and polar cap height anomalies associated with each composite. For three of the ENSO definitions, we also explore the sensitivity of the polar cap effect of ENSO to composite size. We thereby objectively assess the robustness of ENSO teleconnections to the composite size and precise index used.

We first consider whether the tropospheric response to CPW is robust. Figure 3 shows the late winter 300hPa height anomalies associated with each reanalysis ENSO composite. While some CPW composites suggest that CPW leads to a NP trough further south of that associated with EPW (Figure 3c-d), others suggest little robust extratropical response to CPW (Figure 3e-f). In contrast, both EPW composites suggest that EPW leads to a significantly deeper NP trough.

The polar stratospheric response to CPW is not robust. To demonstrate this, we show, in figure 4, the wintertime evolution of anomalous polar cap geopotential height (defined in section 2) for each of these composites. Consistent with previous work (e.g. Manzini et al. [2006], Zubiaurre and Calvo [2012]), the positive geopotential height anomaly in EPW propagates downwards in time (Figure 4a-b). Seasonal mean EPW anomalies are significant at the 95% level, as in Garfinkel and Hartmann [2007]. Figure 4c-f shows the polar response for a wide range of CPW definitions. The responses in the CPW composites are weaker than the responses in the EPW composites (Figure 4a-b). While some CPW composites suggest that CPW strengthens the seasonal mean vortex (Figure 4ef, as in Figure 10 of Hegyi and Deng [2011]), other CPW composites suggest that the seasonal mean vortex is weakened by CPW. Finally, none of the CPW anomalies shown in Figure 4c-f are significant at the 90% level.

The number of winters composited as CPW differs among Hegyi and Deng [2011], Xie et al. [2012], Graf and Zanchettin [2012], and Zubiaurre and Calvo [2012]. The threshold between CPW and neutral ENSO events (or EPW events) is ultimately subjective, and we therefore wish to explore sensitivity to this choice. ENSO composites are created for three different composite sizes for three ENSO definitions: Niño1+2, Modoki, and Nin4>Nin3. As the composite size is increased, moderate El Niño events (or borderline EPW/CPW events) are included. Note that the SST anomalies are qualitatively similar and do not lose their coherence as we increase our composite size (not shown). The polar cap anomalous geopotential height for each index and composite size is shown in Figure 5. The anomalies during EPW are robust to composite size (Figure 5a,d,g). In contrast, the anomalies during CPW are not. For a smaller composite size, CPW as defined by the Modoki index appears to lead to a weakened vortex, but the effect is less apparent when weaker CPW events are included (Figure 5b,e,h). An alternative composite of CPW events would suggest that CPW leads to strengthening of the vortex re-

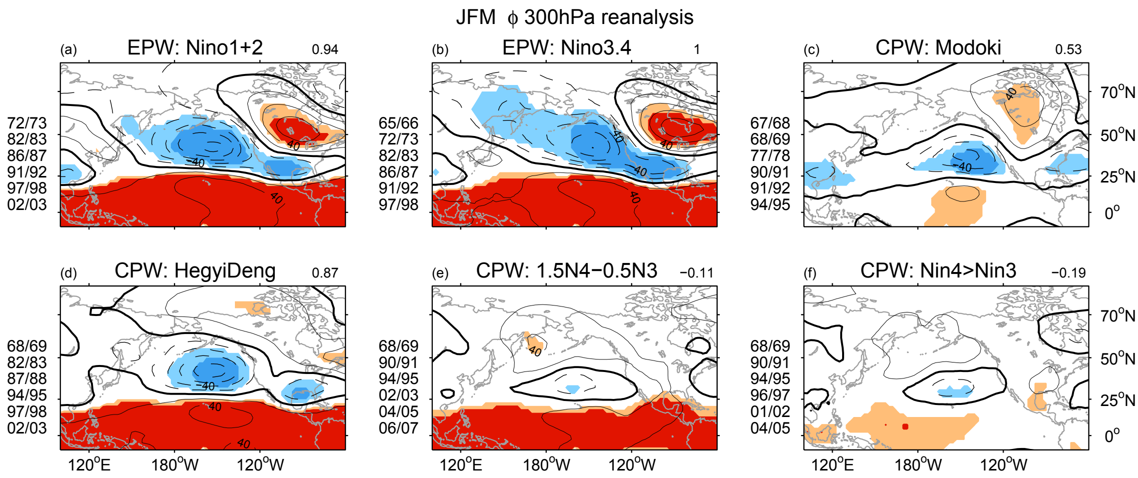

Fig. 3 Geopotential height anomalies at 300hPa in the reanalysis in late winter associated with each composite of ENSO events. Regions with anomalies significant at the 90% (99%) level are colored orange(red) or light blue (dark blue), and contours are shown at ±20, ±40, ±60, ±80, ±100, ±130, ±160, ±200, ±240m. The pattern correlation between the height anomalies in the Niño3.4 composite and the height anomalies in the other composites is shown.

gardless of composite size (Figure 5c,f,i). Overall, we find that the effect of CPW on the vortex is not robust in the reanalysis data. This lack of robustness if also present if we analyze polar cap temperature instead of geopoential height, restrict our composites to the satellite era only, or use MERRA [Rienecker et al., 2011, not shown].

In summary, the extratropical and stratospheric response to CPW is highly dependent on the CPW definition chosen. The sensitivity to CPW index suggests that caution must be applied before generalizing results from the limited observational record. We therefore turn to the long model experiments introduced in Secton 2.2 in the rest of this paper.

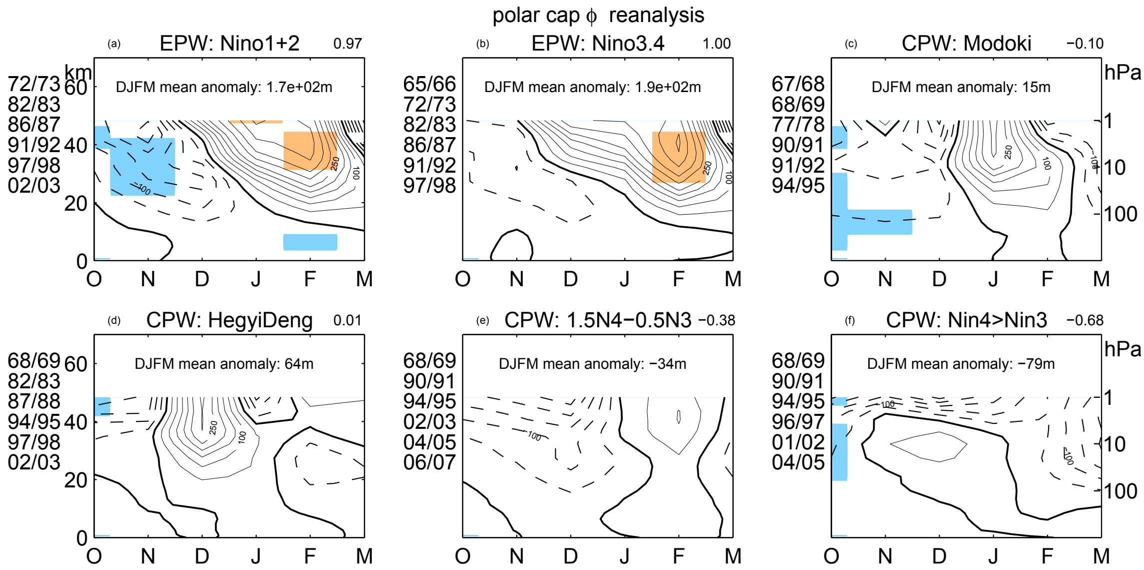

Fig. 4 Polar cap geopotential height anomalies in the reanalysis during ENSO winters. Note that positive polar cap height anomalies indicate a weakened vortex. Regions with anomalies significant at the 90% (99%) level are colored orange(red) or light blue (dark blue) and the contour interval is 50m. The pattern correlation in DJFM between the height anomalies in the Niño3.4 composite and the height anomalies in the other composites is shown. The DJFM seasonal mean 30hPa to 1hPa height anomaly is shown.

4 Perpetual ENSO GEOSCCM Integrations

We now present the response to SSTa in the perpetual CPW and EPW GEOSCCM integrations. The tropospheric response to the SSTa in the Tropics and in the Pacific-North America region are presented in section 4.1 in order to provide context for the stratospheric response. We then examine the stratospheric response in section 4.2.

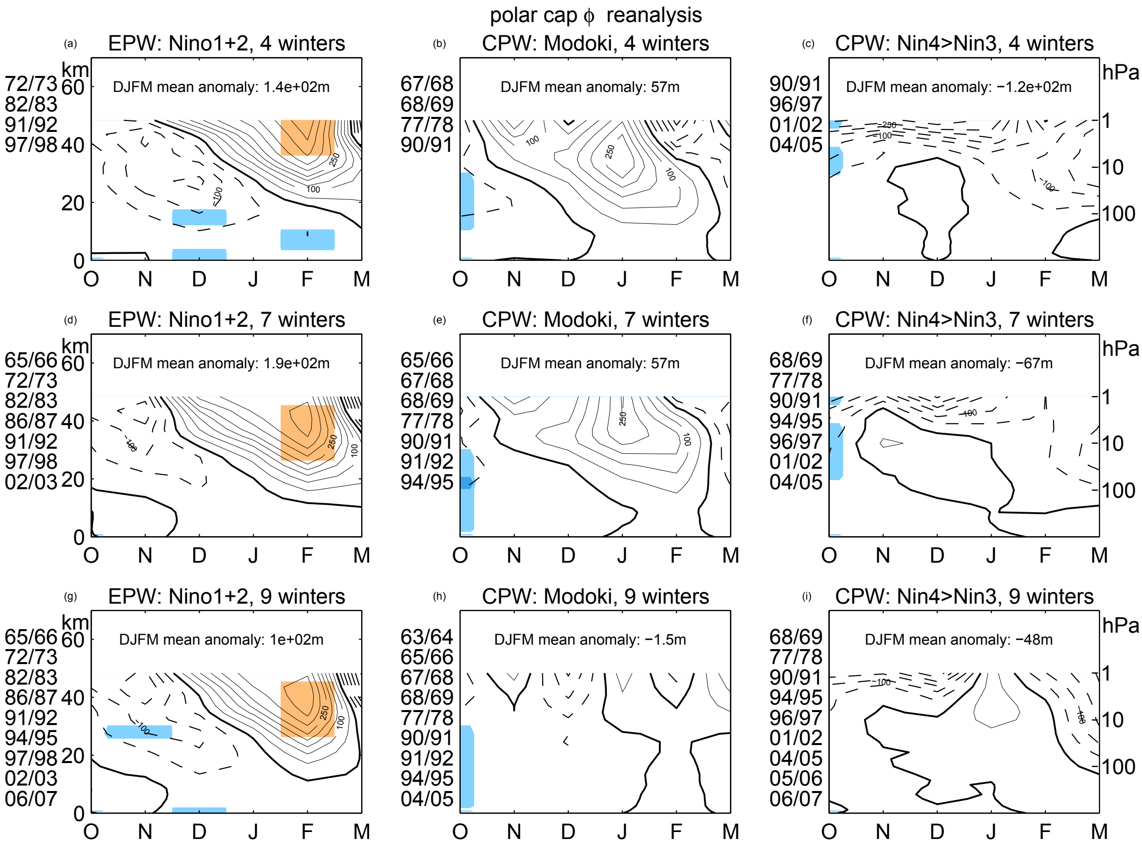

Fig. 5 Polar cap geopotential height anomalies in the reanalysis during ENSO winters for three different ENSO definitions and 3 different composite sizes. Regions with anomalies significant at the 90% (99%) level are colored orange(red) or light blue (dark blue) and the contour interval is 50m. The DJFM seasonal mean 30hPa to 1hPa height anomaly is shown.

4.1 Surface and Tropospheric Response in the Pacific-North America Region

Figure 6 shows anomalies of wintertime precipitation during EPW and CPW. To first order the local response of convection to CPW and EPW are similar- convection is increased in the deep Tropics in the Central Pacific. Nevertheless, there are subtle differences between the EPW and CPW responses (Figures 6g,h). EPW leads to increased precipitation in both the Eastern and Central Tropical Pacific, while CPW leads to increased precipitation mainly in the Central Tropical Pacific. In addition, the magnitude of the increase in Tropical Central Pacific convection is similar for both CPW and EPW in late winter, though not in early winter. These differences are consistent with the stronger and eastward displaced SSTa during EPW than during CPW, though the differences are smaller than the difference in the underlying SSTa forcing (Figure 2 vs. Figure 6). In the extratropics,

1. Precipitation over Western North America is significantly different between EPW and CPW (Figure 6g,h). EPW leads to more precipitation over the Northwestern United States and British Columbia, while CPW leads to more precipitation over Mexico. These anomalies in precipitation over the Western United States appear to be consistent with Figure 11 of Ashok et al. [2007] and Figure 3 of Weng et al. [2009].
2. During EPW, precipitation is increased over East China and decreased over the Philippines, while CPW has a weaker effect on East China precipitation, as in Feng et al. [2010]. However, the anomalies during CPW are generally stronger than Feng et al. [2010] suggests.

Overall, these differences between CPW and EPW are consistent with, though smaller than, those shown in e.g. Ashok et al. [2007], Kug et al. [2009], Feng et al. [2010], and Weng et al. [2009]. The anomalies during CPW and CPWideal are nearly identical outside of the tropical Eastern Pacific.

Figure 7 and 8 show the 2m (i.e. surface) temperature and sea level pressure (SLP) responses to EPW and CPW. Surface temperatures over the tropical oceans follow the anomalous SSTs imposed. To first order the remote response to CPW and EPW are similar - temperatures are anomalously warm over northwestern North America and SLP is anomalously low in the NP. The SLP anomalies during CPW and CPWideal are essentially identical, and the surface temperature anomalies are nearly identical over land (the SSTa in the extratropics differ between the CPW and CPWideal experiments, and so the surface temperature anomalies over oceans should differ). Nevertheless, there are some subtle differences between EPW and CPW teleconnections.

1. In the Tropics, a seasaw pattern in SLP is clear in both EPW and CPW; namely sea level is rising over the eastern Pacific and sinking in the western Pacific (Figure 8a-f). Associated with these SLP anomalies are anomalies in the low-level wind (not shown). These changes are consistent with the Walker Cell changes. This effect is stronger and eastward shifted during EPW as compared to CPW. Nevertheless, the anomalies during EPW and CPW are more similar than those e.g. in Kug et al. [2009].
2. SLP anomalies near Alaska are more strongly negative for EPW than for CPW. Conversely, the anomalous trough extends further into the subtropics (e.g. towards Hawaii) during CPW than during EPW (Figure 8d,e,h). This meridional shifting is similar to, though much weaker than, that noted by Yu and Kim [2011]. Note that the magnitude of the SLP anomaly is similar in both CPW and EPW, however.
3. The surface temperature responses are qualitatively different over the west coast of North America and the far Eastern Pacific. Specifically, temperatures in this region are significantly warmer during CPW than during EPW (Figure 7g,h). This effect appears to be contrary to Figure 12 of Ashok et al. [2007],

though the effect over the West Coast of North America is similar to Figure 11 of Hu et al. [2011]. The southward shift of the warm surface temperature anomaly over North America is consistent with the southward shift of low extratropical SLP during CPW.

Figure 9 shows the 300-hPa height anomalies during early and late winter. To first order the teleconnections of CPW and EPW are similar- heights are anomalously low in the NP. The magnitudes of the NP responses to CPW and EPW are statistically indistinguishable. Nevertheless, the NP low is poleward shifted during EPW as compared to CPW (as in Yu and Kim [2011], Hegyi and Deng [2011], and Zubiaurre and Calvo [2012]). Recall that the NP low was poleward shifted in SLP as well. Finally, a comparison of Figure 8 to 9 suggests that the extratropical tropospheric NP response is barotropic. Finally, the anomalies during CPW and CPWideal are nearly identical

Important differences exist between early and late winter in the strength of the NP teleconnection . Specifically the extratropical response is weaker in early winter and stronger in late winter even though the tropical surface temperature anomalies (and SSTa) are stronger in early winter. The difference between the early winter and late winter responses is statistically significant at the 99% level and is present at the surface as well (e.g., warming over North America and negative SLP anomaly over the NP). The stronger response in JFM is consistent with Frederiksen and Branstator [2005] who find that changes in the extratropical background state associated with the seasonal cycle state lead to larger eddy growth rates in late winter and early spring than in late fall. Changes in the background state encountered by a Rossby wavetrain lead to anomalous extratropical growth in response to the QBO [Garfinkel and Hartmann, 2010] and doubled CO_2 [Meehl et al., 2006] as well.

In summary, CPW (whether idealized or not) and EPW lead to generally similar teleconnections in the Pacific-North America region in GEOSCCM, but differences between CPW and EPW (where they exist) are generally consistent with, though weaker than, those shown in previous studies. We expect that regional seasonal forecasts could be improved if information about these teleconnections was incorporated. We now consider the simulated stratospheric response to CPW and EPW.

4.2 Stratospheric Response

Figure 10 highlights the polar response to ENSO in the troposphere and stratosphere. In late winter both EPW and CPW lead to a weakened vortex, with the magnitude of the effect statistically indistinguishable between the two integrations (Figure 10d). The associated polar cap temperature anomaly exceeds 5K in the lower stratosphere (not shown). The weaker responses in early winter are consistent with the weaker upper tropospheric height anomalies. In both the CPW and EPW experiments, the vortex anomaly propagates downwards in time, reaches the troposphere in FM, and projects onto the negative phase of the NAO, consistent with Graf and Zanchettin [2012] but opposite Hegyi and Deng [2011] (not shown). The negative NAO phase is significantly stronger during CPW than during EPW even though the seasonal mean stratospheric response is weaker, also like in Graf and Zanchettin [2012]. While Graf and Zanchettin [2012] interpret the stronger tropospheric response in CPW, despite a weaker seasonal-mean stratospheric vortex, to mean that the stratosphere does not play an active role in El Niño teleconnections, Figures 4 and 10 suggest that the downward extension of stratospheric anomalies into the troposphere is present in both. We caution that the factor(s) that govern the downward propagation of vortex anomalies from the lower stratosphere into the troposphere are a topic of ongoing work [e.g. Garfinkel et al., 2012b, Mitchell et al., 2012], and that the ability of a stratospheric anomaly to reach the surface is not always related to its amplitude.

The effects of CPW and EPW differ in the upper stratosphere in early winter (ND). Namely, EPW begins to weaken the polar vortex in November (as in Manzini et al. [2006]), while CPW does not. The difference between EPW and CPW is statistically significant in December. The anomalies during CPW and CPWideal are generally similar, though there does appear to be a stronger fall response in CPWideal. Overall, however, the effects of EPW and CPW in the polar stratosphere are similar in that both weaken the vortex.

Garfinkel and Hartmann [2007], Calvo et al. [2009], Garfinkel and Hartmann [2010], Hurwitz et al. [2011a], and Xie et al. [2012] find that the polar atmospheric response to ENSO is sensitive to QBO phase. We have examined whether such an effect is present in our experiments, but we find that the difference in ENSO's effect between EQBO and WQBO is less than 20% and is thus not shown. Both CPW or EPW weaken the vortex regardless of QBO phase, unlike in Xie et al. [2012]. The discrepancy between our studies could arise either because the nonlinearity associated with the QBO is sensitive to the precise SSTa forcing (e.g. the SSTa used in the experiments of Garfinkel and Hartmann [2010] and Xie et al. [2012] differ from ours), or because the effect of the QBO is model-dependent (e.g., Hurwitz et al. [2011b] found no sensitivity to the QBO in the SH in GEOSCCM in the CPW experiment).

Occasionally, the polar vortex completely breaks down, whereby zonal winds change from strong, climatological (>50m/s) westerlies to easterlies in the span of a week at 60N, 10hPa. Such events are known as major stratospheric sudden warmings (SSWs), and are preceded by a burst of wave activity from the troposphere into the stratosphere [Matsuno, 1971]. A SSW can influence tropospheric and surface climate variability in the weeks or months following an event [Polvani and Waugh, 2004, Limpasuvan et al., 2004]. 3.2 SSW occur per decade in the NTRL experiment, 4.7 SSW occur per decade in the CPW experiment, 6.5 occur per decade in the CPWideal experiment, and 7 SSW occur per decade in the EPW experiment [as compared to ∼6 per decade in the observational record, Charlton and Polvani, 2007]. Using a Monte Carlo test to count SSWs in 10,000 random winters equal to the length of the GEOSCCM runs (i.e. 50 years), the probability that the increase in SSW frequency during CPW relative to the NTRL experiment occurred by chance is less than 10% ($p < 0.1$). In the CPWideal experiment, the increase in SSW frequency as compared to the NTRL experiment is statistically significant at the 99% threshold. (The difference between CPW and CPWideal is significant at the 95% threshold. This difference may be due to the presence of warm North Pacific SSTa in the CPW experiment, for Hurwitz et al. [2012] show that such anomalies can reduce SSW frequency.) Both CPW and EPW lead to more frequent SSW relative to NTRL in GEOSCCM. (SSW frequency in the observational record agree with those suggested by GEOSCCM: 3 of the 4 CPW composites suggest 5 SSW occur per decade during CPW, and the fourth suggests

3.33 events per decade. See Garfinkel et al. [2012a] for a thorough discussion of EPW and SSWs.)

4.3 Surface Temperature Response over Europe and in the Global Average

In our GEOSCCM experiments, CPW leads to the negative phase of the NAO, consistent with Graf and Zanchettin [2012] but opposite Hegyi and Deng [2011]. We now explore the subsequent tropospheric impacts of this effect. We then consider the globally averaged surface temperature response to CPW. Associated with the change in the NAO and polar vortex are changes in surface temperature over Eurasia. For example, Graf and Zanchettin [2012] found (1) high latitude Eurasian temperatures are colder during El Niño, and in particular during CPW events as opposed to EPW events and (2) that the effect is largest in Western Eurasia. The area weighted average Western Eurasian surface temperature anomaly is computed and shown in Table 2. During early winter, CPW has little effect on Eurasian temperatures, while EPW does have a significant impact. During late winter, after the stratospheric anomalies have developed, temperatures are colder during both CPW and EPW as compared to the ENSO neutral experiment, and the effects are statistically significant. The impact of EPW on OND Eurasian surface temperature is greater than that of CPW, though in late winter the responses are statistically indistinguishable, unlike in Graf and Zanchettin [2012]. We have also examined the region highlighted in Thompson et al. [2002], and find similar results. The responses in the CPW experiment and in the CPWideal experiment (in which North Atlantic SSTa are identically zero) are similar, highlighting the key role of the stratosphere in producing these surface temperature anomalies. Finally, we

Eurasian Surface Temperature

	OND	JFM
EPW-NTRL	**-0.15**K	-0.13K
CPW-NTRL	0.00K	**-0.15**K
CPWideal-NTRL	0.02K	**-0.20**K

Table 2 Effect of CPW and EPW on Eurasian sector averaged land temperature in the GEOSCCM perpetual ENSO experiments, in Kelvin. The Eurasia sector is defined as land areas poleward of 40°N and between 0°E and 120°E [the region with the largest anomalies due to CPW as shown by Graf and Zanchettin, 2012]. Results are not sensitive to the region chosen, however. Results significant at the 95% level are in bold.

have examined the surface temperature impact in the reanalysis in this region, and we find that it is very sensitive to the precise CPW definition chosen (not shown).

Finally, we consider the impact of CPW index on globally averaged surface temperature, first in the reanalysis and then in GEOSCCM. Table 3 compares the globally averaged surface temperature anomalies in JFM for each ENSO definition. We remove the linear trend in globally averaged surface temperature (i.e. global warming) before computing anomalies. However, results are similar if we do not remove the trend, though composites that sample earlier in the record tend to be colder. The increase in globally averaged temperature during El Niño is robust to the ENSO index used to select events, is quantitatively similar to that reported in Mann and Park [1994], and is present during both EPW and CPW events.

In GEOSCCM, CPW and EPW differ in their impact on globally averaged surface temperature. Global surface temperature is 0.20K higher during CPW (in both the CPWideal and the CPW experiments) than during EPW, and this difference is statistically significant at the 99% level. Even though the globally averaged

Global Surface Temperature, Reanalysis

EPW: Nino1+2	0.05K
EPW: Nino3.4	0.06K
CPW: Modoki	0.01K
CPW: HegyiDeng	0.07K
CPW: 1.5N4-0.5N3	0.02K
CPW: Nin4>Nin3	0.06K

Table 3 Effect of CPW and EPW on globally averaged surface temperature. Surface temperature anomalies have been de-trended before composites are formed.

SSTs used to force the EPW experiment are 0.10K warmer than those of the CPW experiment (and 0.12K warmer than those of the CPWideal experiment), surface temperature is significantly colder. Much of the increase during CPW relative to EPW is from warming in Africa and South America; these continents are warmed by both CPW and EPW, but the warming during CPW is significantly larger than during EPW. We emphasize that each model experiment is identical except for the SST and sea ice climatology used to force the model. The difference in globally averaged surface temperature among the experiments must therefore be an atmospheric response to the imposed SSTa. These model results therefore suggest that the atmospheric response to the precise distribution of SSTs can have an important impact on the global surface temperature response to ENSO. Furthermore, our model results suggest that the observed increase in globally averaged surface temperature during El Niño [e.g Halpert and Ropelewski, 1992, Kumar et al., 1994] is mainly associated with CPW, not EPW. However, model configurations with a coupled ocean will be needed before this result can be stated with more certainty.

In addition, we note that both EPW and CPW lead to anomalously high globally averaged surface temperature in the reanalysis record (cf. Table 3).

4.4 summary

In summary, both CPW and EPW lead to an increase in convection in the deep Tropics, an anomalous low in the NP, and a weakening of the polar stratospheric vortex in late winter. Nearly all of the anomalies during CPW are directly associated with the anomalies in the central Pacific. Our model results suggest that the responses to CPW and EPW are more similar than previously suggested by Hegyi and Deng [2011] and Xie et al. [2012] in the polar vortex region.

5 Variability within CPW

It was shown in Section 3 that the effect of CPW on the vortex in the reanalysis record is very sensitive to the CPW index used and the number of winters included. While some of this sensitivity is likely due to differences in the underlying SSTa (i.e. the SSTa in Figure 1 differ among the CPW composites), some of it is due to internal variability and the limited record length. To quantify the minimum composite size necessary before the signal due to CPW rises above the noise, we examine the length of integration necessary before the weakening of the vortex in the perpetual CPW GEOSCCM experiment becomes robust.

Figures 11a-b illustrate how internal variability can mask the polar stratospheric response to CPW events. Geopotential height anomalies in the four winters with the strongest vortices in the 50-year simulation have the opposite sign as those in the four winters with the weakest vortices. Even though the difference

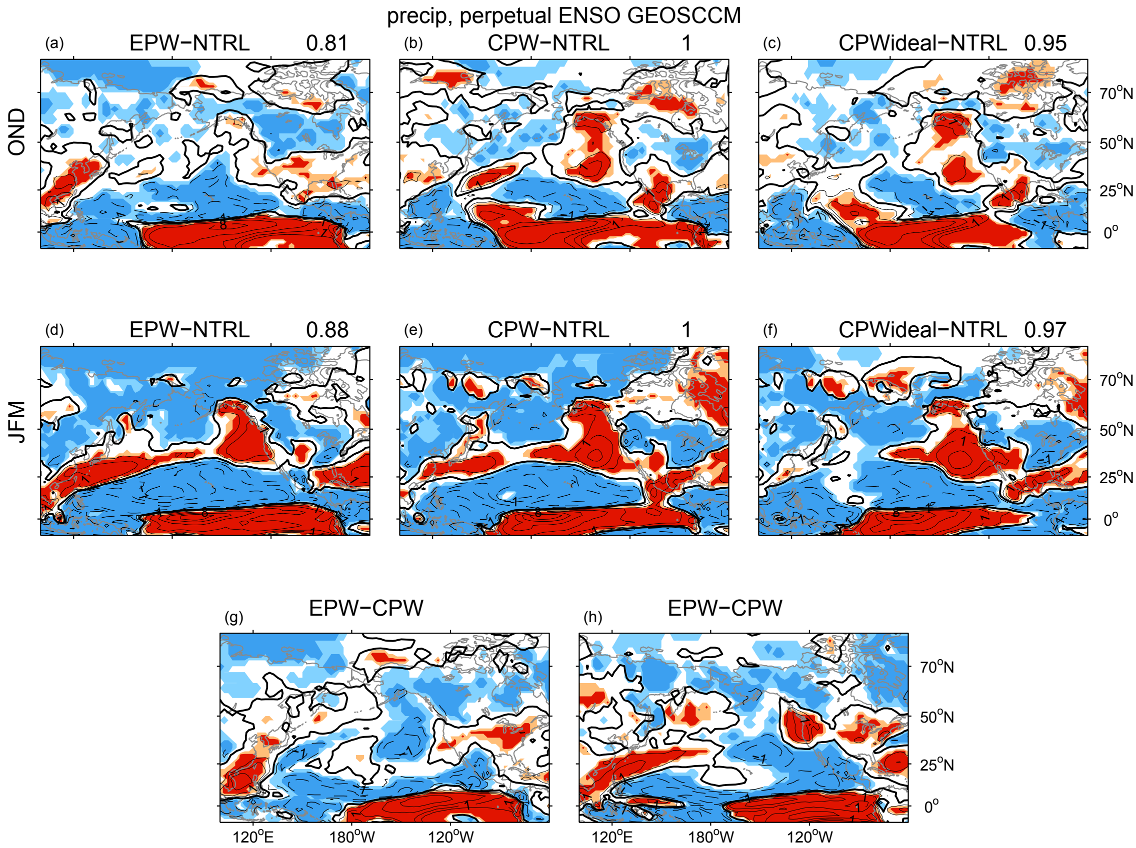

Fig. 6 Precipitation anomalies in the perpetual ENSO GEOSCCM integrations. Contours are shown at ±.5, ±1, ±2, ±4, ±8 mmday^{-1}, and regions with anomalies significant at the 90% (99%) level are colored orange(red) or light blue (dark blue). The zero line is bolded. (a)-(c) and (g) are for early winter (OND) and (d)-(f) and (h) are for late winter. (g),(h) compare the EPW and CPW integrations. The pattern correlation between the CPW and EPW anomalies are shown in the title of (a)-(f).

in late winter vortex strength between the CPW and ENSO neutral experiments is statistically significant at the 99.999% level, substantial intra-CPW variability can mask the effect of anomalous CPW SST.

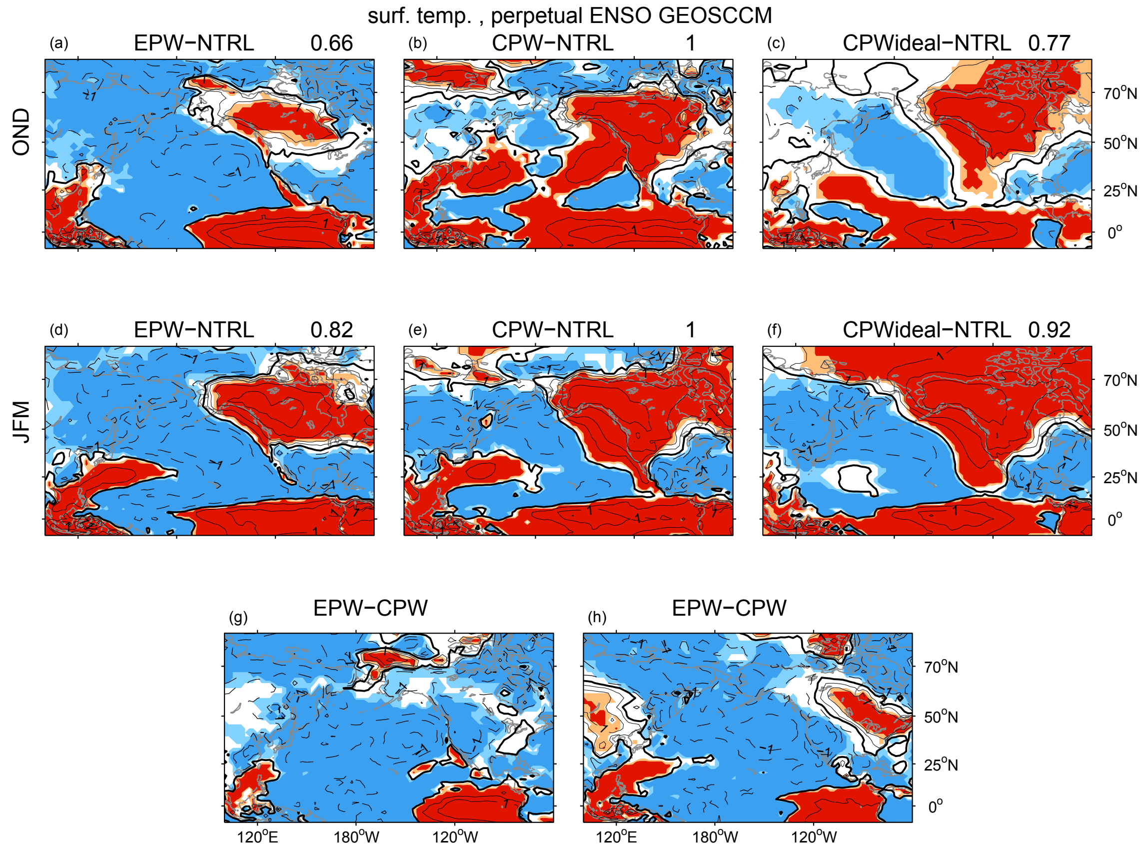

Fig. 7 Like Figure 6 but for 2meter (i.e. surface) temperature anomalies. Contours are shown at ±.5, ±1, ±2, ±4, ±8K.

We now assess the relative probability of an anomalously strong vortex in a four year composite of CPW events by the following Monte Carlo test. 10,000 four year subsamples of the CPW GEOSCCM integrations are selected randomly, and the probability distribution function of DJFM 1hPa-30hPa polar cap height anomalies in the 10,000 member ensemble is shown in Figure 11c. It is clear that a wide range of polar cap anomalies are possible in a four year subsample. Approximately 3% of the subsamples show a strengthening of the vortex. A similar Monte

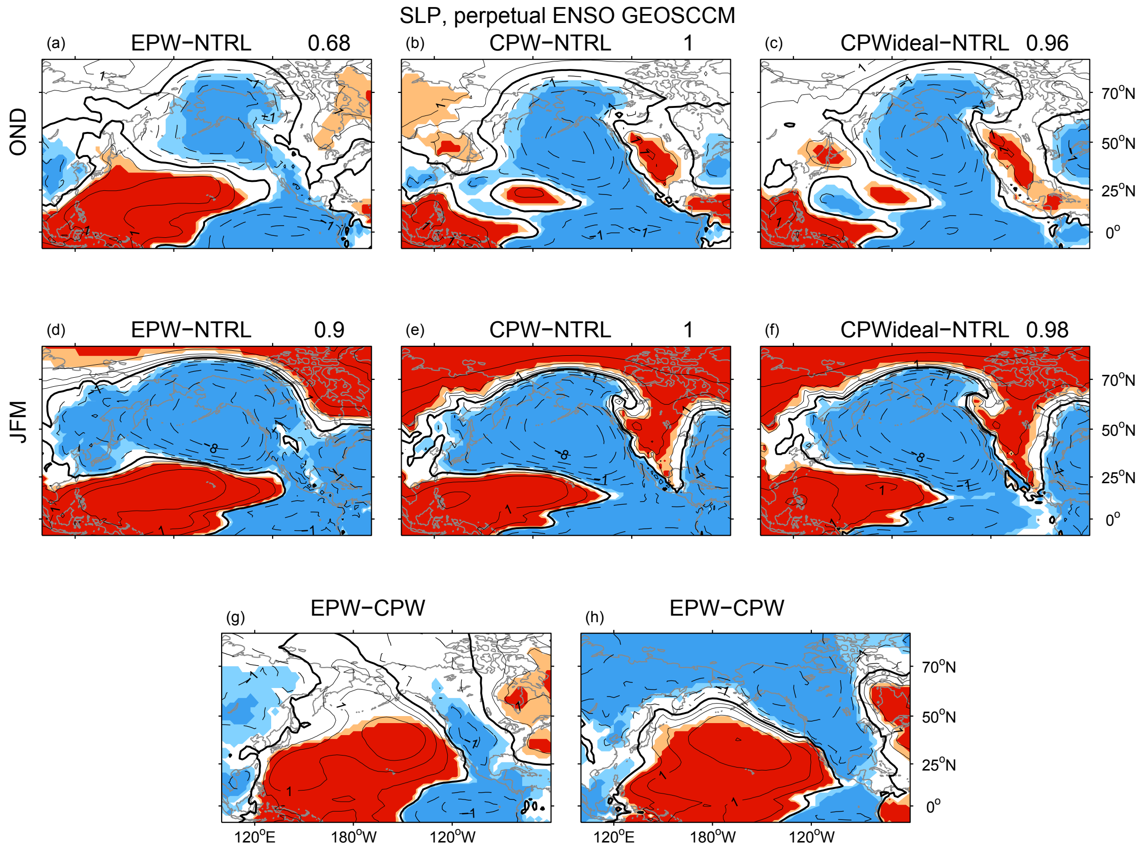

Fig. 8 Like Figure 6 but for sea level pressure anomalies. Contours are shown at ±0.5, ±1, ±2, ±4, ±8, and ±16hPa.

Carlo test but with six year subsamples (as in Figure 1 and 4) suggests that 1% of the subsamples might show a strengthening of the vortex. Figure 11d considers how long an integration is needed before the difference between CPW and neutral ENSO becomes statistically significant. Specifically, 10,000 random subsamples of the CPW and neutral ENSO experiment are selected, and the statistical significance of their difference is computed. We then evaluate the percentage of the 10,000 differences that exceed the 95% and 99% confidence levels as a function of

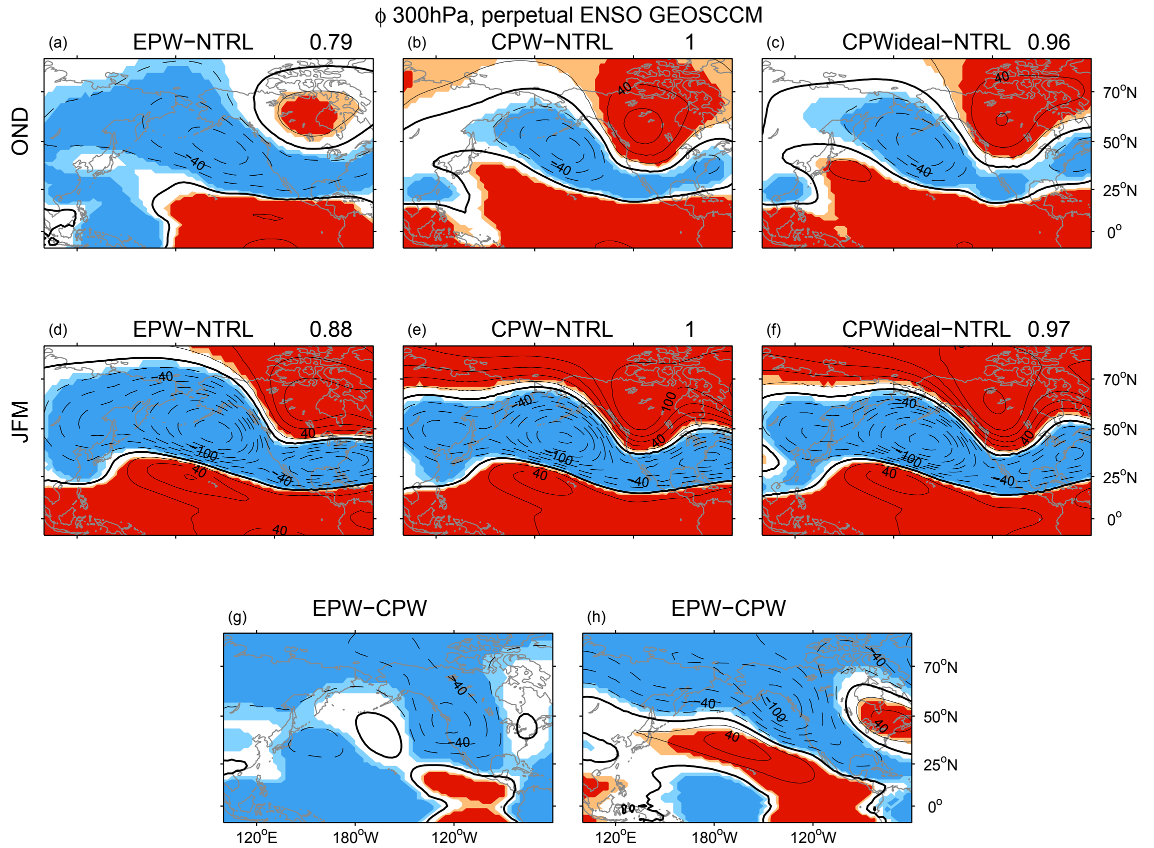

Fig. 9 Like Figure 6 but for geopotential height anomalies at 300hPa. Contours are shown at ±20, ±40, ±60, ±80, ±100, ±130, ±160, ±200, ±240m.

the number of years included in each subsample. 95% of GEOSCCM integrations 16(21) years long would have suggested that the effect of CPW on the vortex is significantly different from that neutral ENSO at the 95% (99%)level. While the precise minimum integration length is almost certainly model-dependent, these results suggests that long simulations are necessary in order to isolate the impact of ENSO from internal variability.

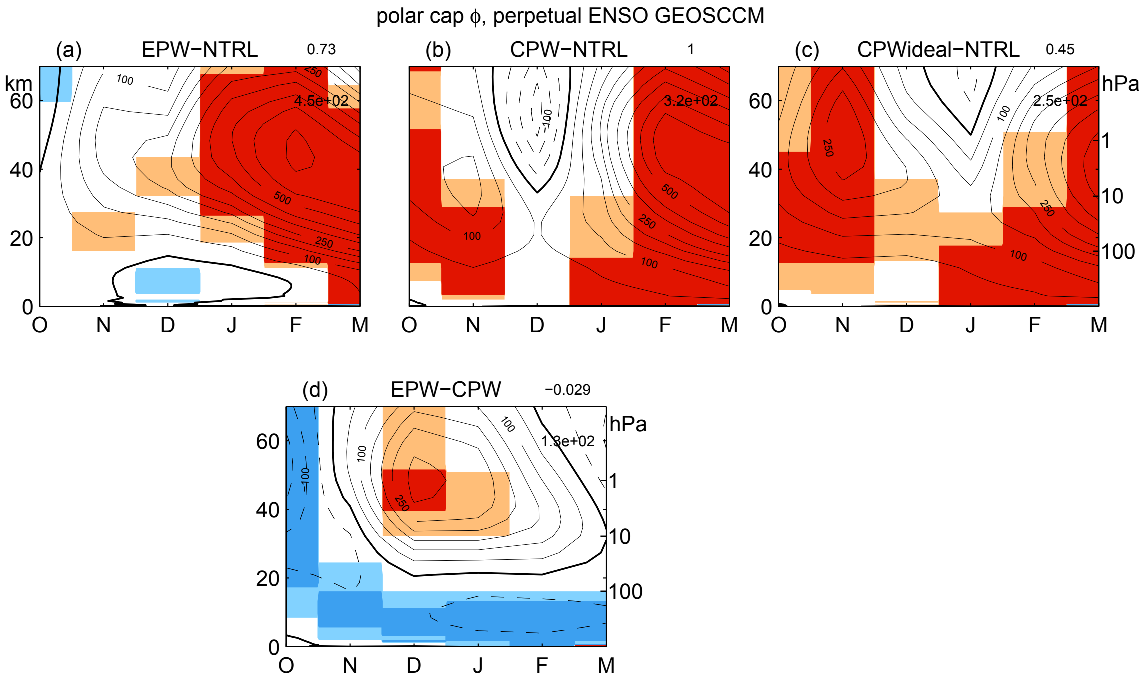

Fig. 10 Polar cap (i.e. the area weighted average from 70N and poleward) geopotential height in the perpetual ENSO GEOSCCM integrations during the extended winter season. Regions with anomalies significant at the 90% (99%) level are colored orange(red) or light blue (dark blue), and contours are shown at ±50, ±100, ±150, ±200, ±250, ±325, ±400, ±500, ±600, and ±750m. DJFM seasonal mean anomaly is shown inside each panel, and the DJFM pattern correlation with the CPW anomalies is shown for (a) and (c).

6 Discussion and Conclusions

The ERA-40 reanalysis and simulations of the Goddard Earth Observing System Chemistry-Climate Model, Version 2 (GEOS V2 CCM) are used to compare the teleconnections in the Pacific-North America region and stratosphere associated with Central Pacific El Niño (CPW) and (canonical) eastern Pacific El Niño (EPW). In the reanalysis data, we find that the effect of CPW in the Pacific-North

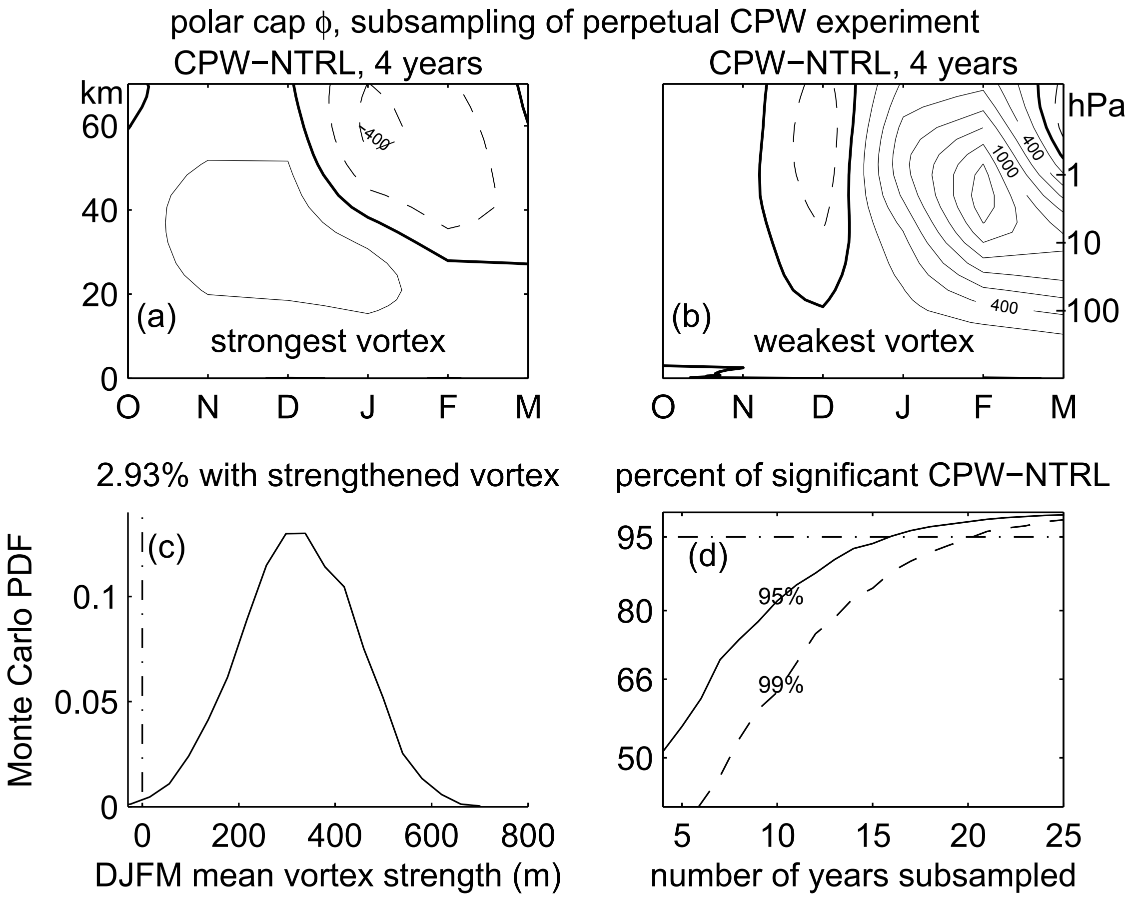

Fig. 11 Polar cap geopotential height anomalies in the GEOSCCM CPW experiment (a) in the four winters with the strongest vortex, and (b) in the four winters with the weakest vortex. Contour interval is ±200m. (c) Probability distribution function of 1hPa-30hPa polar cap height anomalies in 4 year subsamples of the CPW GEOSCCM integrations. (d) Monte Carlo test of the integration length necessary before the difference between CPW and neutral ENSO becomes significant at the 95% and 99% confidence levels (see text for details).

America region is sensitive to the index used to define Central Pacific warming, the number of winters included in a composite, and the month within the extended winter season. This sensitivity highlights that caution must be applied before generalizing results from the limited observational record.

The long model integrations indicate that in boreal winter, the teleconnections of CPW and EPW are generally the same. Namely, both EPW and CPW lead to a deepened NP low and a weakened polar vortex, and the effects are stronger in late winter than in early winter. However, differences do exist between the two forms of El Niño. CPW shifts westward the Tropical response as compared to canonical El Niño. In addition, the structure of the Tropical Pacific warming appears to be important for understanding the impact of El Niño on surface temperature and precipitation over North America and sea level pressure over the subtropical Pacific. In particular, the NP trough is displaced slightly poleward for EPW as compared to CPW. In addition, the polar stratospheric response in December is significantly stronger during EPW than during CPW. Finally, the GEOSCCM runs suggest that CPW results in a larger increase of globally averaged surface temperature than EPW. These differences are generally consistent with, though weaker than, those shown in previous work. These results regarding CPW and EPW teleconnections may be of use towards improving regional seasonal forecasts.

The similarity of the extratropical response to EPW and CPW is perhaps not surprising. Prescribed SST anomalies cause local changes in the low-level temperatures, winds, and humidity, which in turn lead to local precipitation anomalies. The equatorial waves associated with the upper level divergence anomalies from the local precipitation anomalies spreads the influence throughout the Tropics [Gill, 1980, Jin and Hoskins, 1995]. The resulting local and non-local divergence anomalies then force a Rossby wave train that propagates to the extratropics [Hoskins and Karoly, 1981, Sardeshmukh and Hoskins, 1988]. This Rossby wave can then interact with the extratropical mean flow and eddies and can thereby be amplified [Simmons et al., 1983, Held et al., 1989, Garfinkel and Hartmann, 2010]. This theory would suggest that if the tropical precipitation anomalies (which we take as a proxy for divergence) associated with El Niño are similar for CPW and EPW (which they are in GEOSCCM), then the extratropical tropospheric response (and subsequent stratospheric response) should be similar. In addition, the similarity of the responses in the default CPW experiment and the idealized CPW experiment in which cold SSTa are present in the tropical Eastern Pacific (as in the experiments of Xie et al. [2012]) suggests that central Pacific anomalies are of paramount importance for the extratropical response. The overall similarity among the responses appears to be consistent with the idealized modeling studies of Geisler et al. [1985], Barsugli and Sardeshmukh [2002].

The aforementioned theory does not appear to be capable of connecting the slight zonal shift in tropical precipitation with the poleward or equatorward shift of the extratropical NP low (and the subsequent impacts on North America) however, and we are not aware of any explanation of this poleward shift in previous work. We speculate that it could be related to linear wave propagation. Namely, Hoskins and Ambrizzi [1993, their equation 2.11] show that the radius of curvature of a Rossby wave propagating into the extratropics is proportional to its zonal wavelength. As the convective source is more zonally confined during CPW and the subsequent wavelength of the extratropical Rossby wave is shorter, we might expect that the radius of curvature will be smaller and therefore for the wave to not reach as high a latitude. A thorough test of this explanation for the latitude of the North Pacific response is left for future work.

In contrast to the NH, in the Southern Hemisphere there is a qualitative difference between the extratropical teleconnections associated with central and eastern Pacific warming. Namely, CPW significantly impacts the South Pacific Convergence Zone while EPW does not [Hurwitz et al., 2011a,b]. It is therefore expected that only CPW can modify planetary waves in the SH troposphere and thereby influence the SH polar vortex [Hurwitz et al., 2011a,b, Zubiaurre and Calvo, 2012]. Weakening of the vortex in SH springtime Hurwitz et al. [2011a] is robust to the four definitions of CPW presented in this paper. Preliminary results also indicate that the Pacific-North America teleconnections of CPW and EPW are more distinct in summertime (when the subtropical jet is weak) than in wintertime in our GEOSCCM experiments; additional analysis is left for future work. However, our GEOSCCM experiments indicate that in the wintertime Northern Hemisphere, warming focused in either the central or eastern Pacific leads to a similar extratropical response.

Garfinkel et al. [2012a] show that the representation of NH El Niño teleconnections in GEOSCCM is generally quite good. However, the complexity of the sequence of physical events leading from SST forcing to atmospheric response raises questions about any conclusions based on an individual atmospheric GCM (for example, EPW teleconnections in the SH are biased in this model). Future work with additional models is necessary to confirm the findings in this study. Nevertheless, we suggest the following:

1. While the teleconnection patterns of central and eastern Pacific warming are subtly distinct, both tend to weaken the late winter Northern Hemisphere polar vortex.
2. Care must be taken when choosing the index used to identify central Pacific warming.
3. The early winter responses to central and eastern Pacific warming are distinct from the late winter responses.
4. At least 20 years of model output data (and likely a similar number of observed events) are needed before robust conclusions can be drawn regarding the nature of the stratospheric response to central Pacific warming.

7 Appendix

Figure 12 shows the month-by-month evolution of 300hPa height anomalies in GEOSCCM. The response to EPW and CPW in December is qualitatively weaker than the response in January. The response in March is as strong as the response in January or February. The difference between the early winter and late winter responses is statistically significant at the 99% level. Compositing OND together and JFM together appears to be justified.

Acknowledgements This work was supported by the NASA grant number NNX06AE70G and NASA's ACMAP program.

References

K. Ashok, S. K. Behera, S. A. Rao, H. Weng, and T. Yamagata. El Niño Modoki and its possible teleconnection. *Journal of Geophysical Research (Oceans)*, 112:

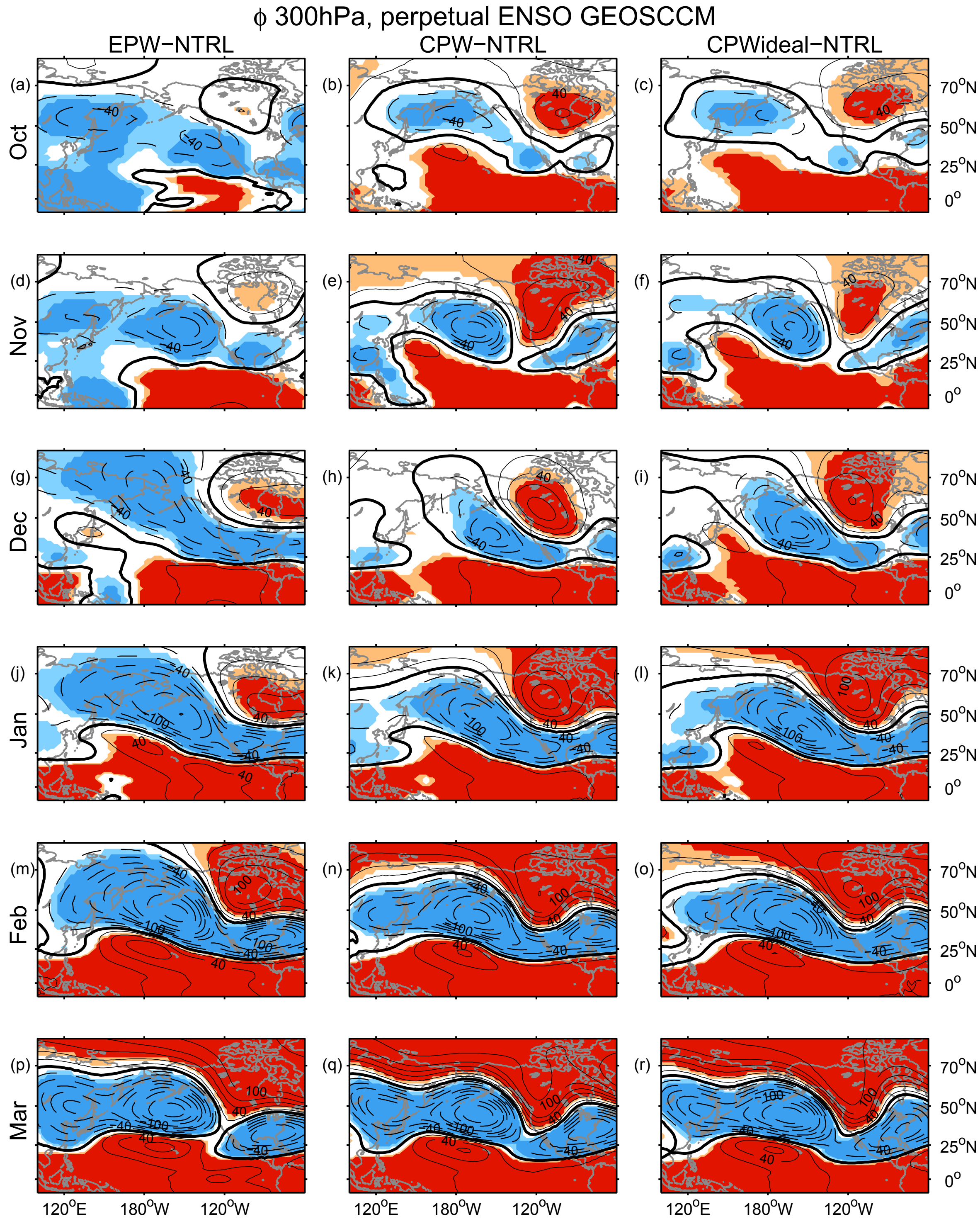

Fig. 12 Geopotential height anomalies at 300hPa in the perpetual ENSO GEOSCCM integrations in each extended winter month. Contours are shown at ±20, ±40, ±60, ±80, ±100, ±130, ±160, ±200, ±240m, and regions with anomalies significant at the 90% (99%) level are colored orange(red) or light blue (dark blue).

C11007, November 2007. doi: 10.1029/2006JC003798.

A. G. Barnston, A. Kumar, L. Goddard, and M. P. Hoerling. Improving Seasonal Prediction Practices Through Attribution of Climate Variability. *Bulletin of the American Meteorological Society*, 86:59–72, January 2005. doi: 10.1175/BAMS-86-1-59.

J. J. Barsugli and P. D. Sardeshmukh. Global atmospheric sensitivity to tropical sst anomalies throughout the indo-pacific basin. *J. Clim.*, 15:3427?3442, 2002.

C. J. Bell, L. J. Gray, A. J. Charlton-Perez, M. M. Joshi, and A. A. Scaife. Stratospheric Communication of El Niño Teleconnections to European Winter. *Journal of Climate*, 22:4083–+, 2009. doi: 10.1175/2009JCLI2717.1.

C. Cagnazzo, E. Manzini, N. Calvo, A. Douglass, H. Akiyoshi, S. Bekki, M. Chipperfield, M. Dameris, M. Deushi, A. Fischer, H. Garny, A. Gettelman, M. A. Giorgetta, D. Plummer, E. Rozanov, T. G. Shepherd, K. Shibata, A. Stenke, H. Struthers, and W. Tian. Northern winter stratospheric temperature and ozone responses to ENSO inferred from an ensemble of Chemistry Climate Models. *Atmospheric Chemistry & Physics Discussions*, 91:12141–12170, May 2009.

N. Calvo, M. A. Giorgetta, R. Garcia-Herrera, and E. Manzini. Nonlinearity of the combined warm enso and qbo effects on the northern hemisphere polar vortex in maecham5 simulations. *J. Geophys. Res.*, 114(D13109), July 2009. doi: 10.1029/2008JD011445.

A. J. Charlton and L. M. Polvani. A New Look at Stratospheric Sudden Warmings. Part I: Climatology and Modeling Benchmarks. *Journal of Climate*, 20:449–+, 2007. doi: 10.1175/JCLI3996.1.

J. Feng, L. Wang, W. Chen, S. K. Fong, and K. C. Leong. Different impacts of two types of Pacific Ocean warming on Southeast Asian rainfall during boreal winter. *J. Geophys. Res.*, 115, 2010. doi: 10.1029/2010JD014761.

J. S. Frederiksen and G. Branstator. Seasonal Variability of Teleconnection Patterns. *Journal of Atmospheric Sciences*, 62:1346–1365, May 2005. doi: 10.1175/JAS3405.1.

C. I. Garfinkel and D. L. Hartmann. Effects of the El-Nino Southern Oscillation and the Quasi-Biennial Oscillation on polar temperatures in the stratosphere. *J. Geophys. Res.- Atmos.*, 112:D19112, 2007. doi: 10.1029/2007JD008481.

C. I. Garfinkel and D. L. Hartmann. Different ENSO teleconnections and their effects on the stratospheric polar vortex. *J. Geophys. Res.- Atmos.*, 113, 2008. doi: 10.1029/2008JD009920.

C. I. Garfinkel and D. L. Hartmann. The influence of the quasi-biennial oscillation on the north pacific and el-niño teleconnections. *J. Geophys. Res.*, 115:D20116, 2010. doi: 10.1029/2010JD014181.

C. I. Garfinkel, D. L. Hartmann, and F. Sassi. Tropospheric precursors of anomalous northern hemisphere stratospheric polar vortices. *J. Clim.*, 23, 2010.

C. I. Garfinkel, A. H. Butler, D. W. Waugh, and M. M. Hurwitz. Why might SSWs occur with similar frequency in El Niño and La Niña winters? *J. Geophys. Res.*, in press, 2012a. doi: 10.1029/2012JD017777.

C.I. Garfinkel, D. W. Waugh, and E.P. Gerber. Effect of tropospheric jet latitude on coupling between the stratospheric polar vortex and the troposphere. *J. Clim.*, in press, 2012b.

J. E. Geisler, M. L. Blackmon, G. T. Bates, and S. Muñoz. Sensitivity of January Climate Response to the Magnitude and Position of Equatorial Pacific Sea Surface Temperature Anomalies. *Journal of Atmospheric Sciences*, 42:1037–1049, May 1985. doi: 10.1175/1520-0469(1985)042⟨1037:SOJCRT⟩2.0.CO;2.

A. E. Gill. Some simple solutions for heat-induced tropical circulation. *Quarterly Journal of the Royal Meteorological Society*, 106:447–462, July 1980. doi: 10.1002/qj.49710644905.

H. Graf and D. Zanchettin. Central Pacific El Nino, the subtropical bridge, and eurasian climate. *J. Geophys. Res.*, 117, 2012. doi: 10.1029/2011JD016493.

M. S. Halpert and C. F. Ropelewski. Surface Temperature Patterns Associated with the Southern Oscillation. *Journal of Climate*, 5:577–593, June 1992. doi: 10.1175/1520-0442(1992)005⟨0577:STPAWT⟩2.0.CO;2.

B. Hegyi and Y. Deng. A dynamical fingerprint of tropical Pacific sea surface temperatures in the decadal-scale variability of the cool-season Arctic precipitation. *J. Geophys. Res.*, 2011.

I. M. Held, S. W. Lyons, , and S. Nigam. Transients and the extratropical response to El Nino. *J. Atmos. Sci.*, 46(1):163–174, 1989.

M. P. Hoerling, A. Kumar, and M. Zhong. El Niño, La Nina, and the nonlinearity of their teleconnections. *J. Clim.*, 10:1769–1786, 1997.

J. D. Horel and J. M. Wallace. Planetary scale atmospheric phenomena associated with the Southern Oscillation. *Mon. Weather Rev.*, 109:813–829, 1981.

B. J. Hoskins and T. Ambrizzi. Rossby wave propagation on a realistic longitudinally varying flow. *J. Atmos. Sci.*, 50:1661–1671, 1993. doi: 10.1175/1520-0469(1993)050.

B. J. Hoskins and D. Karoly. The steady linear response of a spherical atmosphere to thermal and orographic forcing. *J. Atmos. Sci.*, 38:1179–1196, 1981.

Z. Hu, A. Kumar, B. Jha, W. Wang, B. Huang, and B. Huang. An analysis of warm pool and cold tongue el niños: airsea coupling processes, global influences, and recent trends. *Climate Dynamics*, pages 1–19, 2011. ISSN 0930-7575. doi: 10.1007/s00382-011-1224-9.

M.M. Hurwitz, P.A. Newman, L.D. Oman, and A.M. Molod. Response of the Antarctic stratosphere to two types of El Niño events. *J. Atmos. Sci.*, 68:812–822, 2011a. doi: 10.1175/2011JAS3606.1.

M.M. Hurwitz, I.-S. Song, L.D. Oman, P.A. Newman, A.M. Molod, S.M. Frith, and J.E. Nielsen. Response of the Antarctic stratosphere to warm pool El Niño events in the GEOS CCM. *Atmos. Chem. Phys.*, 11:9659–9669, 2011b. doi: 10.5194/acp-11-9659-2011.

M.M. Hurwitz, P.A. Newman, and C.I. Garfinkel. On the Influence of North Pacific Sea Surface Temperatures on the Arctic Winter Climate. *J. Geophys. Res.*, in press, 2012. doi: 10.1029/2012JD017819.

S. Ineson and A. A. Scaife. The role of the stratosphere in the European climate response to El Nino. *Nature-Geo*, 2:32 – 36, 2009. doi: 10.1038/ngeo381.

F. Jin and B. J. Hoskins. The direct response to tropical heating in a baroclinic atmosphere. *J. Atmos. Sci.*, 52:307–319, February 1995. doi: 10.1175/1520-0469(1995)052.

H.-Y. Kao and J.-Y. Yu. Contrasting Eastern-Pacific and Central-Pacific Types of ENSO. *Journal of Climate*, 22:615, 2009. doi: 10.1175/2008JCLI2309.1.

J.-S. Kug, F.-F. Jin, and S.-I. An. Two Types of El Niño Events: Cold Tongue El Niño and Warm Pool El Niño. *Journal of Climate*, 22:1499, 2009. doi: 10.1175/2008JCLI2624.1.

A. Kumar, A. Leetmaa, and M. Ji. Simulations of Atmospheric Variability Induced by Sea Surface Temperatures and Implications for Global Warming. *Science*, 266:632–634, October 1994. doi: 10.1126/science.266.5185.632.

N. K. Larkin and D. E. Harrison. Global seasonal temperature and precipitation anomalies during El Niño autumn and winter. *Geophys. Res. Lett.*, 32:L16705, August 2005. doi: 10.1029/2005GL022860.

V. Limpasuvan, D. W. J. Thompson, and D. L. Hartmann. The life cycle of the Northern Hemisphere sudden stratospheric warmings. *J. Clim.*, 17:2584–2596, 2004.

M. E. Mann and J. Park. Global-scale modes of surface temperature variability on interannual to century timescales. *J. Geophys. Res.*, 99:25819–25834, December 1994. doi: 10.1029/94JD02396.

E. Manzini, M. A. Giorgetta, L. Kornbluth, and E. Roeckner. The influence of sea surface temperatures on the northern winter stratosphere: Ensemble simulations with the MAECHAM5 model. *J. Clim.*, 19:3863–3881, 2006.

T. Matsuno. A dynamical model of the stratospheric sudden warming. *J. Atmos. Sci.*, 1971.

G. A. Meehl, H. Teng, and G. Branstator. Future changes of El Niño in two global coupled climate models. *Climate Dynamics*, 26:549–566, May 2006. doi: 10.1007/s00382-005-0098-0.

D.M. Mitchell, L.J. Gray, M.P Baldwin, A.J Charlton-Perez, and J. Anstey. The influence of stratospheric vortex displacements and splits on surface climate. *J. Clim.*, submitted, 2012.

K. Nishii, H. Nakamura, and Y. J. Orsolini. Cooling of the wintertime Arctic stratosphere induced by the western Pacific teleconnection pattern. *Geophys. Res. Lett.*, 371:L13805, July 2010. doi: 10.1029/2010GL043551.

L. M. Polvani and D. W. Waugh. Upward wave activity flux as a precursor to extreme stratospheric events and subsequent anomalous surface weather regimes. *Journal of Climate*, 17:3548–3554, 2004.

N. A. Rayner, D. E. Parker, E. B. Horton, C. K. Folland, L. V. Alexander, D. P. Rowell, E. C. Kent, and A. Kaplan. Global analyses of sea surface temperature, sea ice, and night marine air temperature since the late nineteenth century. *Journal of Geophysical Research (Atmospheres)*, 108:4407, July 2003. doi: 10.1029/2002JD002670.

H.-L. Ren and F.-F. Jin. Niño indices for two types of ENSO. *Geophys. Res. Lett.*, 380:L04704, February 2011. doi: 10.1029/2010GL046031.

M. M. Rienecker, M. J. Suarez, R. Gelaro, R. Todling, J. Bacmeister, E. Liu, M. G. Bosilovich, S. D. Schubert, L. Takacs, G.-K. Kim, S. Bloom, J. Chen, D. Collins, A. Conaty, A. da Silva, W. Gu, J. Joiner, R. D. Koster, R. Lucchesi, A. Molod, T. Owens, S. Pawson, P. Pegion, C. R. Redder, R. Reichle, F. R. Robertson, A. G. Ruddick, M. Sienkiewicz, and J. Woollen. MERRA: NASA's Modern-Era Retrospective Analysis for Research and Applications. *Journal of Climate*, 24:3624–3648, July 2011. doi: 10.1175/JCLI-D-11-00015.1.

C. F. Ropelewski and M. S. Halpert. Global and Regional Scale Precipitation Patterns Associated with the El Niño/Southern Oscillation. *Monthly Weather Review*, 115:1606, 1987. doi: 10.1175/1520-0493(1987)115⟨1606:GARSPP⟩2.0.CO;2.

P. D. Sardeshmukh and B. J. Hoskins. The generation of global rotational flow by steady idealized tropical divergence. *J. Atmos. Sci.*, 45:1228–1251, 1988.

J. Shukla, J. Anderson, D. Baumhefner, C. Brankovic, Y. Chang, E. Kalnay, L. Marx, T. Palmer, D. Paolino, J. Ploshay, S. Schubert, D. Straus, M. Suarez, and J. Tribbia. Dynamical Seasonal Prediction. *Bulletin of the American Meteorological Society*, 81:2593–2606, November 2000. doi: 10.1175/1520-0477(2000)081⟨2593:DSP⟩2.3.CO;2.

A. Simmons, J. M. Wallace, and G. Branstator. Barotropic wave propagation and instability, and atmospheric teleconnection patterns. *J. Atmos. Sci.*, 40:1363–1392, 1983.

SPARC-CCMVal. SPARC Report on the Evaluation of Chemistry-Climate Models. *SPARC Report*, 5, WCRP-132, WMO/TD-No. 1526, 2010. URL `http://www.atmosp.physics.utoronto.ca/SPARC`.

D. W. J. Thompson, M. P. Baldwin, and J. M. Wallace. Stratospheric Connection to Northern Hemisphere Wintertime Weather: Implications for Prediction. *J. Clim.*, 15:1421–1428, 2002. doi: 10.1175/1520-0442(2002)015.

K. E. Trenberth and J. M. Caron. The Southern Oscillation Revisited: Sea Level Pressures, Surface Temperatures, and Precipitation. *Journal of Climate*, 13:4358–4365, December 2000. doi: 10.1175/1520-0442(2000)013⟨4358:TSORSL⟩2.0.CO;2.

K. E. Trenberth and D. P. Stepaniak. Indices of El Niño Evolution. *Journal of Climate*, 14:1697–1701, April 2001. doi: 10.1175/1520-0442(2001)014⟨1697:LIOENO⟩2.0.CO;2.

S. M. Uppala, P. W. Kållberg, A. J. Simmons, U. Andrae, V. da Costa Bechtold, M. Fiorino, J. K. Gibson, J. Haseler, A. Hernandez, G. A. Kelly, X. Li, K. Onogi, S. Saarinen, N. Sokka, R.P. Allan, E. Andersson, K. Arpe, M. A. Balmaseda, A. C. M. Beljaars, L. van de Berg, J. Bidlot, N. Bormann, S. Caires, F. Chevallier, A. Dethof, M. Dragosavac, M. Fisher, M. Fuentes, S. Hagemann, E. Hólm, B. J. Hoskins, L. Isaksen, P. A. E. M. Janssen, R. Jenne, A. P. Mc-

Nally, J. F. Mahfouf, J. J. Morcrette, N. A. Rayner, R. W. Saunders, P. Simon, A. Sterl, K. E. Trenberth, A. Untch, D. Vasiljevic, P. Viterbo, and J. Woollen. The ERA-40 reanalysis. *Quart. J. Roy. Meteorol. Soc.*, 2005.

H. Weng, S. K. Behera, and T. Yamagata. Anomalous winter climate conditions in the Pacific rim during recent El Niño Modoki and El Niño events. *Climate Dynamics*, 32:663–674, April 2009. doi: 10.1007/s00382-008-0394-6.

F. Xie, J. P. Li, W. S. Tian, and J. Feng. Signals of el niño modoki in the tropical tropopause layer and stratosphere. *Atmos. Chem. Phys.*, 12:D, 2012. doi: 10.5194/acp-12-5259-2012.

S.-W. Yeh, J.-S. Kug, B. Dewitte, M.-H. Kwon, B. P. Kirtman, and F.-F. Jin. El Niño in a changing climate. *Nature*, 461:511–514, September 2009. doi: 10.1038/nature08316.

J.-Y. Yu and H.-Y. Kao. Decadal changes of ENSO persistence barrier in SST and ocean heat content indices: 1958-2001. *Journal of Geophysical Research (Atmospheres)*, 112:D13106, July 2007. doi: 10.1029/2006JD007654.

J.-Y. Yu and S. T. Kim. Relationships between Extratropical Sea Level Pressure Variations and the Central Pacific and Eastern Pacific Types of ENSO. *Journal of Climate*, 24:708–720, February 2011. doi: 10.1175/2010JCLI3688.1.

I. Zubiaurre and N. Calvo. The El Nino–Southern Oscillation (ENSO) Modoki signal in the stratosphere. *J. Geophys. Res.*, 117, 2012. doi: 10.1029/2011JD016690.